Electronic Supporting Information

Terminal Moiety-Driven Electrical Performance of Asymmetric Small-Molecule Based Organic Solar Cells

Jianhua Huang,[a] *Shanlin Zhang,*[b] *Bo Jiang,*[b] *Yuxia Chen,*[b] *Xinliang Zhang,*[b] *Zhuxin Fan,*[a] *Donghong Yu,*[c,d] *Zhiyong Lin,*[a] *Jiannian Yao,*[b] *Chuanlang Zhan**[b]

[a] College of Materials Science and Engineering, Huaqiao University, Xiamen, 361021, P. R. China; E-mail: huangjh@iccas.ac.cn

[b] Beijing National Laboratory for Molecular Sciences, CAS Key Laboratory of Photochemistry, Institute of Chemistry, Chinese Academy of Sciences, Beijing, 100190, P. R. China; E-mail: clzhan@iccas.ac.cn

[c] Department of Chemistry and Bioscience, Aalborg University, Fredrik Bajers Vej 7H, DK-9220, Aalborg, Denmark; E-mail: yu@bio.aau.dk

[d] Sino-Danish Centre for Education and Research (SDC), Niels Jenses Vej 2, DK-8000, Aarhus, Denmark.

Contents

1. Experimental section

1.1 Measurements and characterizations

The ^{1}H NMR and ^{13}C NMR spectra were obtained on a Bruker AVANCE 400 MHz spectrometer using tetramethylsilane (TMS; δ = 0 ppm) as an internal standard. Mass spectra (MALDI-TOF-MS) were collected on a Bruker BIFLEX III mass spectrometer. Elemental analysis was performed on a flash EA1112 analyzer. UV-vis absorption spectrum was recorded on a Hitachi U-3010 spectrophotometer. The samples were prepared by spin-coating the corresponding chloroform solution on the quartz slides. The electrochemical measurements were carried out in a deoxygenated solution of tetra-n-butylammoniumhexafluorophosphate (0.1 M) in $CHCl_3$ with a computer-controlled Zennium electrochemical workstation. A glassy carbon electrode, a Pt wire, and an Ag/AgCl electrode were used as the working, counter, and reference electrodes, respectively. Atomic force microscope (AFM) images were obtained from the photovoltaic device samples using a Nanoscope V AFM (Digital Instruments) in tapping mode. Transmission electronic microscope (TEM) tests were performed on a JEM-2011F operated at 200 kV. The TEM specimens were prepared by transferring the spin-coated films to the 200 mesh copper grids. The X-ray diffraction(XRD) pattern was recorded by a Rigaku D/max–2500 diffractometer operated at 40 kV voltage and a 200 mA current with Cu Kα radiation. The XRD samples were prepared by spin-coating the corresponding *o*-DCB solution on the silica substrate. The silica substrate was utilized instead of the ITO surfaces to avoid the interference signal of ITO to the sample signal, while both of them are hydrophilic, which should impact less differently on the film-morphology.[1]

1.2 DFT calculations

Density functional theory (DFT) calculations were performed using the Gaussian 09 program[2] with the B3LYP exchange-correlation functional.[3-5] All-electron triple-ξ valence basis sets with polarization functions (6-31G) are used for all atoms. Geometry optimizations were performed with full relaxation of all atoms. All alkyl chains were reduced to methyl groups for avoiding computational load. The initial structure of thiophene-DPP-thiophene was constructed in the gjf input files according to the single crystal data reported in literature.[6] For each molecule, various conformations with different dihedral angles were optimized, and the data for the one with the lowest energy are reported.

1.3 Fabrications and PV tests of organic solar cells

The organic solar cells (OSCs) devices were fabricated with the traditional configurations of ITO/PEDOT: PSS/active layer/Ca/Al. The indium tin oxide (ITO) glass was precleaned, respectively, with deionized water, acetone and isopropanol and treated in a Novascan PSD-ultraviolet-ozone chamber for 30 min. A thin layer (ca. 30 nm) of

poly(3,4-ethylene-dioxythiophene):poly(styrenesulfonate) (PEDOT:PSS, Baytron P VP AI 4083, Germany) was spin-coated onto the ITO glass at 2000 rpm and baked at 150 °C for 10 min. A solution of **M1**/PC71BM, **M2**/PC71BM, **M3**/PC71BM, and **M4**/PC71BM, respectively, with *o*-DCB as solvent and DIO as co-solvent was subsequently spin-coated on the surface of the PEDOT: PSS layer to form a photosensitive layer. Then, the Ca/Al cathode was deposited on the photoactive layer by vacuum evaporation (ca. 20/80 nm). The active area of the device was of 0.06 cm^2. The current-voltage characteristics of all solar cell devices were measured with a Keithley 2400 source and conducted in a nitrogen-filling glove-box. An AM 1.5G solar simulator (AAA grade, XES-70S1) was used as the light source. The light intensity of the solar simulator is calibrated to be 100 mW/cm^2 (at the position of sample) with a standard silicon reference solar cell (Area 20×20 mm^2, the certification of the reference cell is accredited by NIST to the ISO-17025 standard). The EQE measurements were performed using a AC-type 250 W Quartz Tungsten Halogen (Oriel) fitted with a monochromator (Cornerstone (CS130) 1/8m) as a monochromatic light source.

1.4 Tests of hole mobilities

The hole mobilities of the active layer were determined by applying the space charge limited current (SCLC) model to the *J*-*V* tests of hole-only devices. The hole-only devices were fabricated with configuration of ITO/PEDOT: PSS/active layer/Au. The active layers were spin-coated under the same condition to that of device preparation. The Au layer (100 nm) was deposited under a low speed (1 Å/10 s) to avoid the penetration of Au atoms into the active layer. The *J*-*V* curves were tested under dark on a computer-controlled Keithley 2400 Source Measure Unit. **Figure S2** shows current-voltage curve of the hole-only devices corrected by built-in voltage (V_{bi}). It's found that, by assuming V_{bi} = 0.3 V, the injecting current follows a quadratic dependence at high voltage (marked with red line in **Figure S2**) , indicating spacing-charge-limited-conduction in this region. Experimental data in this region were fitted to the Mott-Gurney equation as follows: [7,8]

$$J = (9\mu\varepsilon/8L^3) \times (V\text{-}V_{bi})^2$$

where J the current density, μ the hole mobility, ε the dielectric constant of the organic semiconductors, L the thickness of the films, as specified in **Figure S2**, V the applied potential, and V_{bi} the built-in potential which results from the difference in the work function of the anode and the cathode. The hole mobility of the blending films were deduced from the intercept value $\mathrm{Log}(9\mu\varepsilon/8L^3)$. Herein ε is 3.

1.5 Tests of dipole moments

The experimental dipole moments of **M1**, **M2**, **M3**, **M4**, and PC71BM were tested in diluted solutions. Six n-type solvents, e.g., 2-butanone, acetone, butanenitrile, DMF, DMSO, and acetonitrile with different polarity were selected. Two solvent polarity parameters, BK and Δf, checked from literature are shown in **Table S2** [9]. The dipole moments of **M1**, **M2**, **M3**, **M4** were tested, respectively, as follows:

The sample was dissolved in the six solvents, respectively, and diluted to 10^{-6} M. Absorption maxima (υ_a^{sol}, cm^{-1}), fluorescence emission maxima (υ_a^{sol}, cm^{-1}) and corresponding Stokes shifts

($v_a^{sol} - v_f^{sol}, cm^{-1}$) were tested. A linear fitting of the Stokes shifts ($v_a^{sol} - v_f^{sol}, cm^{-1}$) versus solvent polarity parameter BK were carried out according to the following equation:

$$\nu_a^{sol} - \nu_f^{sol} = \left(\nu_a^{gas} - \nu_f^{gas}\right) + \left[\frac{\left|\mu_e - \mu_g\right|^2}{hca_w^3}\right] BK$$

v is the wavenumber of absorption maximum of the electronic transition of the sample in solution (sol), in gas phase (gas), in absorption and in fluorescence, respectively, μ_g and μ_e are the dipole moments of the ground and excited state, respectively, h the Planck costant, c the speed of light in vacuum, a_w the Onsager radius. a_w = [molecular length (Å)× width (Å) × thickness (Å)]$^{1/3}$ were obtained by the Gaussian calculating results.

The fitted lines were shown in **Figure S5a**. The slopes and relative linear coefficients R2 were shown in **Table S3**. The difference of the ground and excited dipole moments, $\Delta\mu_{eg}$ were estimated by using the slope values of the fitted lines.

Then, another linear fitting of absorption maxima (v_a^{sol}, cm^{-1}) versus Δf was carried out according to the following equation:

$$\nu_f^{sol} = const - \left(\frac{2}{hca_w^3}\right)\left[(\mu_e - \mu_g)\mu_e \Delta f - \frac{\left(\mu_e - \mu_g\right)^2\left(n^2 - 1\right)}{2\left(n^2 + 2\right)}\right]$$

The fitted lines were shown in **Figure S5b**. The ground dipole moments (μ_g) were estimated by using the slope values of the fitted lines. The $\Delta\mu_{eg}$, μ_e, and μ_g were shown in **Table S4**.

2. Supporting Figures and Tables

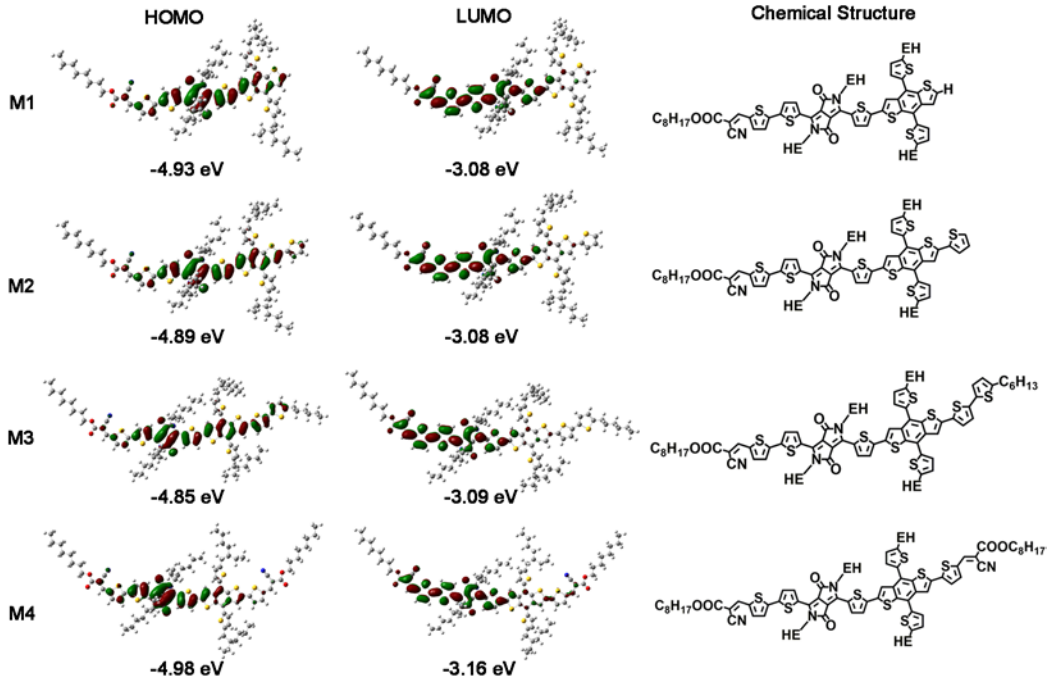

Figure S1. HOHO and LUMO surface plots of **M1**, **M2**, **M3**, and **M4**, respectively, calculated by the DFT methods.

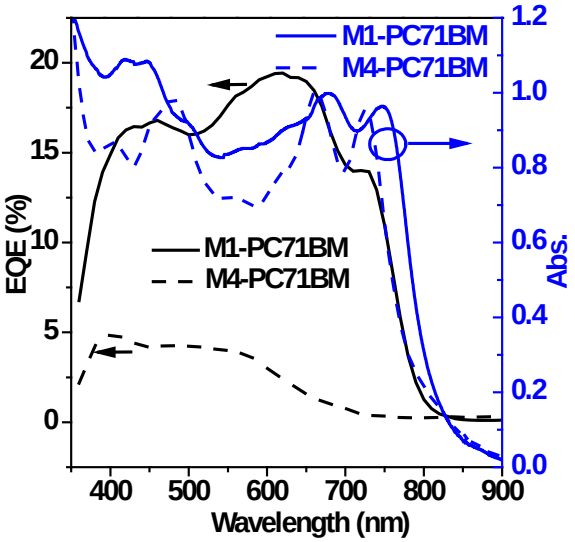

Figure S2. EQE curves and blend film absorption spectrum for **M1** and **M4**, respectively.

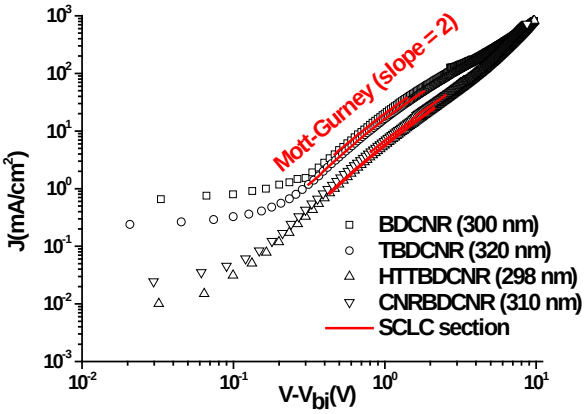

Figure S3. The *J*-*V* curves of the hole-only devices corrected by the built-in potential (V_{bi}). The hole mobilities were calculated by fitting the SCLC sections (red line) to the Mott-Gurney laws.

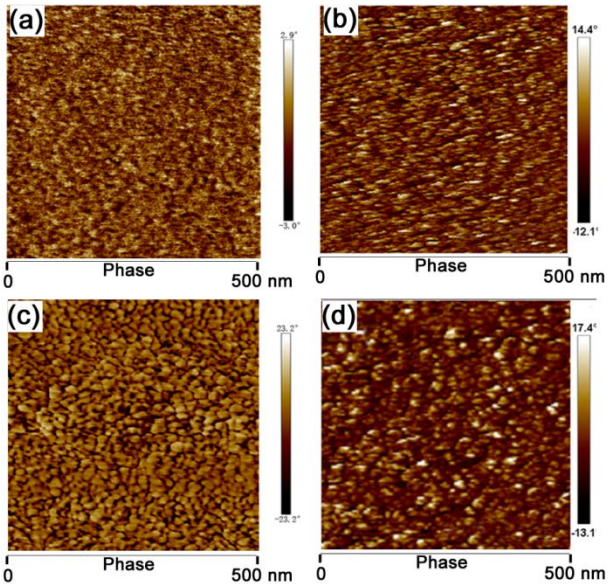

Figure S4. AFM phase images of the **M1**, **M2**, **M3**, and **M4**, respectively blended with PC71BM.

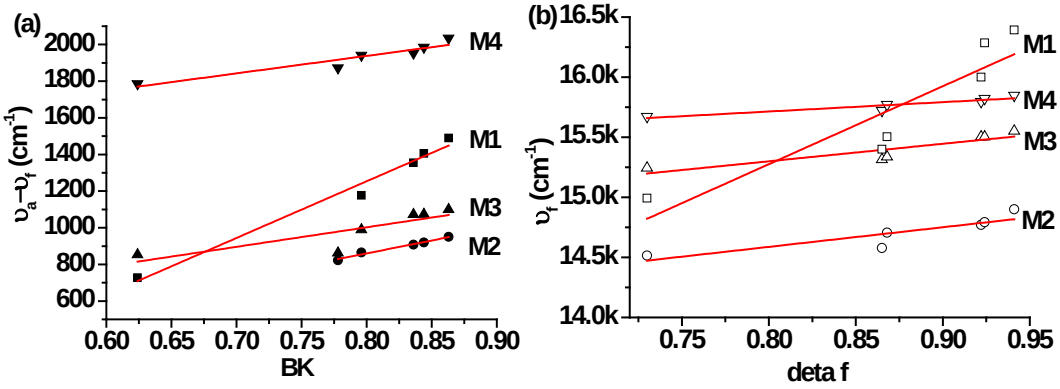

Figure S5. Plots of ($\upsilon_a^{sol} - \upsilon_f^{sol}$) vs. BK (a) and υ_f^{sol} vs. Δf (b), respectively.

Table S1. Parameters of device optimization processes for the four asymmetric molecules with PC71BM as the acceptor material. The average PCEs were derived statistically from ten cells, as shown in the brackets.

	D/A	DIO (v/v%)	PCE (avg %)	J_{sc} (mA/cm^2)	V_{oc} (V)	FF (%)
M1	1:1	0	1.40 (1.35)	4.44	0.84	37.6
		0.1	1.88 (1.84)	5.65	0.81	41.0
		0.2	3.58 (3.48)	7.06	0.82	61.7
		0.3	2.88 (2.82)	6.17	0.80	58.0
		0.4	2.53 (2.45)	5.61	0.81	55.8
		0.5	2.04 (1.99)	5.14	0.76	52.3
		1.0	1.50 (1.40)	4.05	0.75	49.0
	2:1	0.2	2.39 (2.27)	5.31	0.77	58.0
	1:2	0.2	2.25 (2.18)	6.44	0.77	45.4
M2	2:1	0	0.46 (0.39)	1.49	0.81	37.9
		1.0	1.84 (1.80)	3.88	0.76	62.2
	1:1	0	1.12 (1.06)	2.65	0.78	54.0
		0.8	2.76 (2.66)	6.00	0.71	64.7
		1.0	3.06 (3.01)	6.65	0.74	62.3
		1.2	2.52 (2.33)	6.01	0.73	59.0
	1:2	0	0.56 (0.45)	1.92	0.71	37.7
		1.0	1.50 (1.39)	3.77	0.76	52.3
M3	2:1	0	0.47 (0.38)	1.32	0.73	48.6
		1.0	2.30 (2.11)	6.23	0.68	54.0
	1:1	0	0.61 (0.44)	1.53	0.71	56.0
		0.5	1.01 (0.82)	3.64	0.64	43.0
		1.0	2.52 (2.45)	6.45	0.67	58.4
		2.0	1.17 (1.09)	6.06	0.53	36.6
	1:2	0	0.52 (0.45)	1.29	0.74	54.0
M4	2:1	0	0.26 (0.22)	0.82	0.79	41.0
		1.0	0.78 (0.63)	2.35	0.74	45.0
	1:1	0	0.36 (0.33)	0.91	0.78	41.0
		0.5	0.63 (0.58)	1.76	0.77	46.0
		1.0	0.91 (0.83)	2.76	0.78	42.0
	1:2	0	0.15 (0.09)	0.71	0.68	31.0

Table S2. Solvents selected for the tests of dipole moments and the polarity parameters checked from the literature.

Solvents	BK	Δf
2-butanone	0.624	0.730
acetone	0.796	0.868
butanenitrile	0.778	0.865
DMF	0.836	0.922
DMSO	0.844	0.941
acetonitrile	0.863	0.924

Table S3. Slopes and relative linear coefficients R2 for plots of ($v_a^{sol} - v_f^{sol}$) vs. BK and v_f^{sol} vs. Δf, respectively.

	M1		**M2**		**M3**		**M4**	
	slope	R^2	slope	R^2	slope	R^2	slope	R^2
BK	3094	0.98	1408	0.97	1021	0.84	954	0.87
Δf	6489	0.80	1632	0.73	1456	0.75	780	0.83

Table S4. Experimental dipole moments of ground state ($\Delta\mu_g$), excited state ($\Delta\mu_e$)and difference of ground and excited state ($\Delta\mu_{eg}$), respectively.

	$\Delta\mu_{eg}$ (D)	μ_e (D)	μ_g (D)
M1	1.44	0.45	1.89
M2	2.38	0.76	3.14
M3	2.36	0.83	3.19
M4	2.32	1.47	3.79

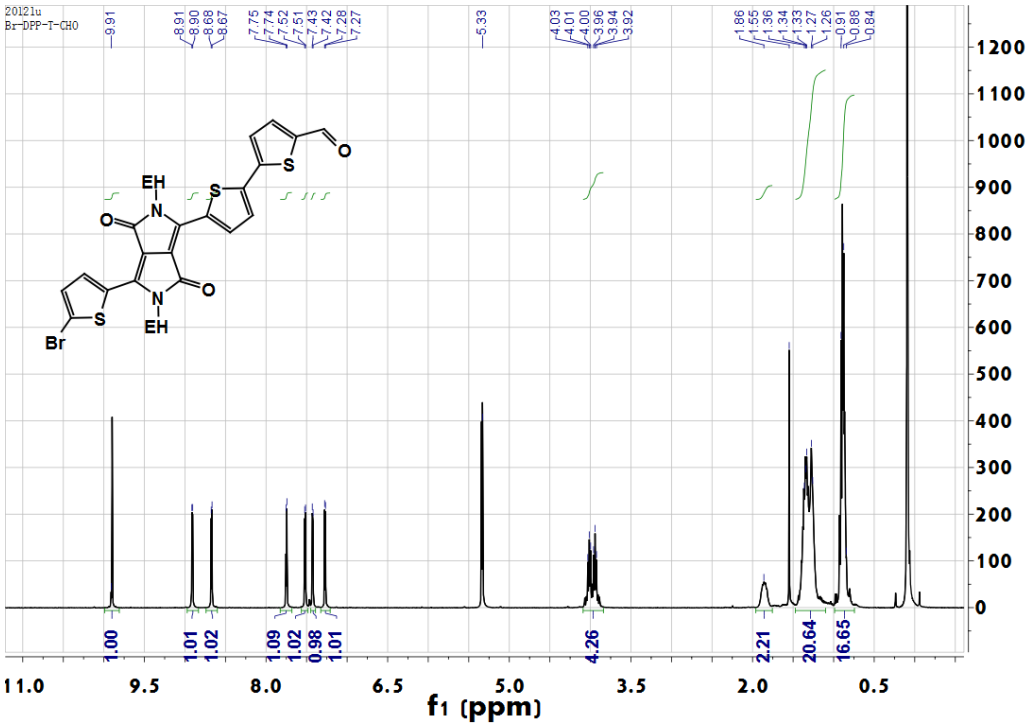

Figure S6. ^{1}H NMR spectrum of compound **3**.

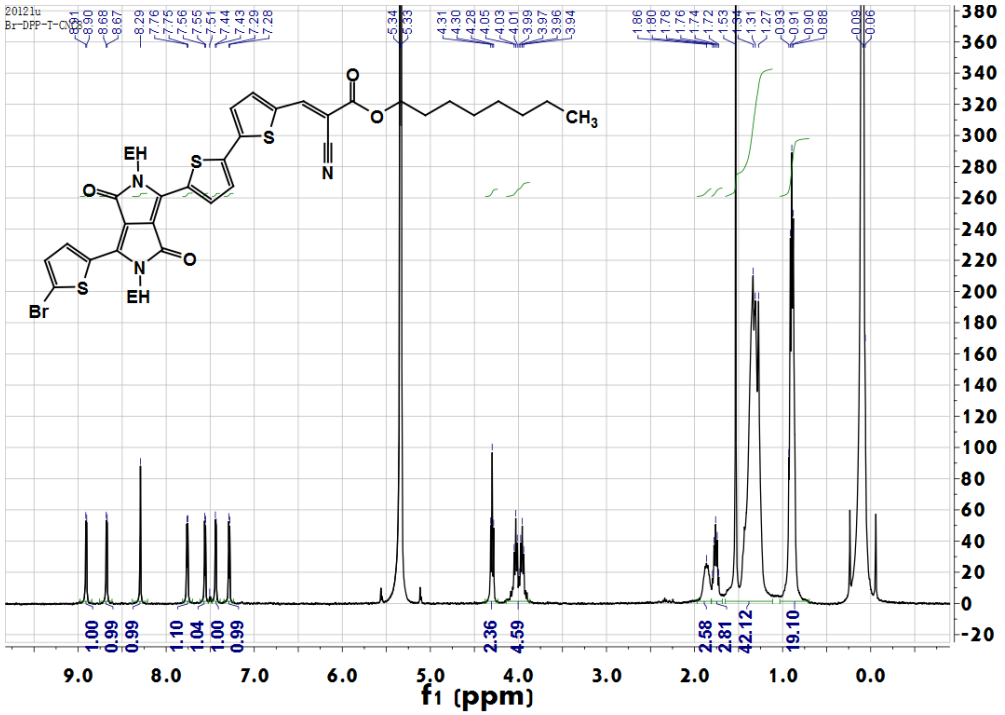

Figure S7. ^{1}H NMR spectrum of compound **5**.

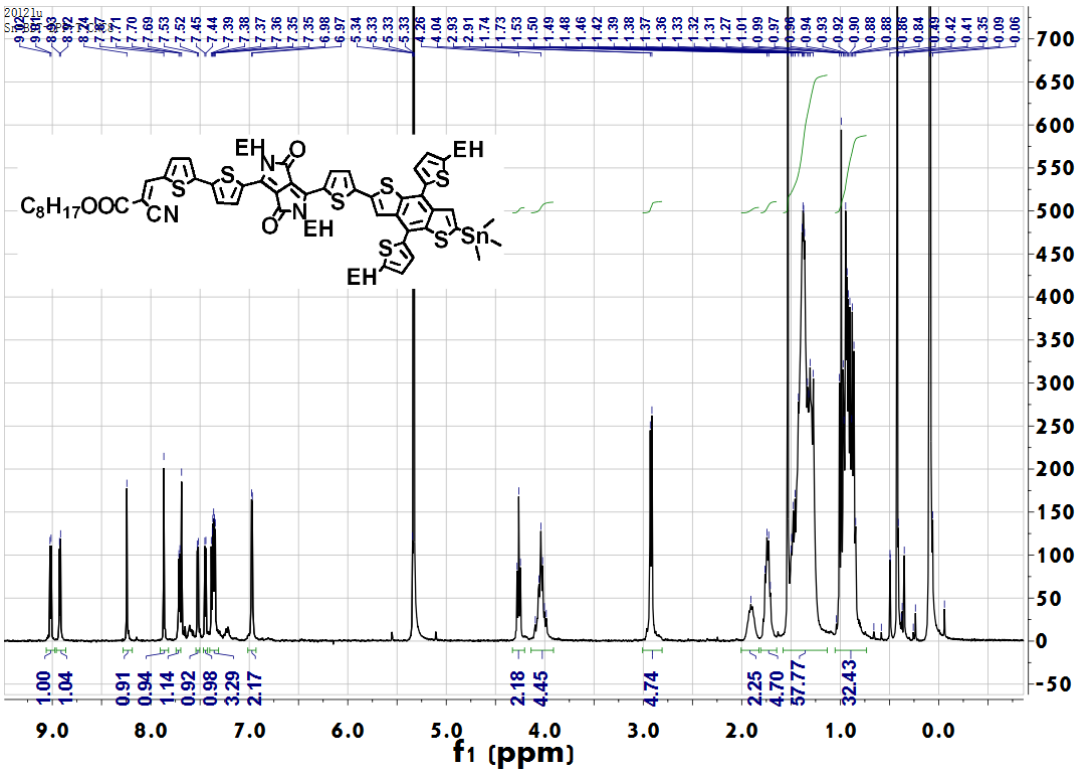

Figure S8. ^{1}H NMR spectrum of compound **10**.

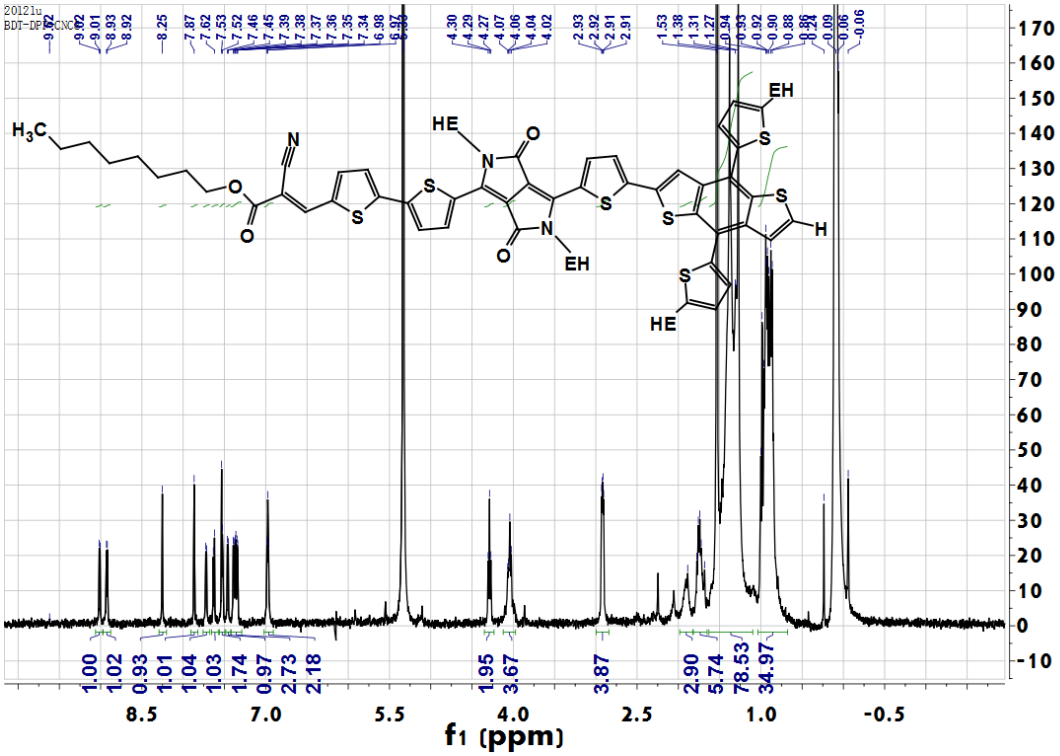

Figure S9. ^{1}H NMR spectrum of **M1**.

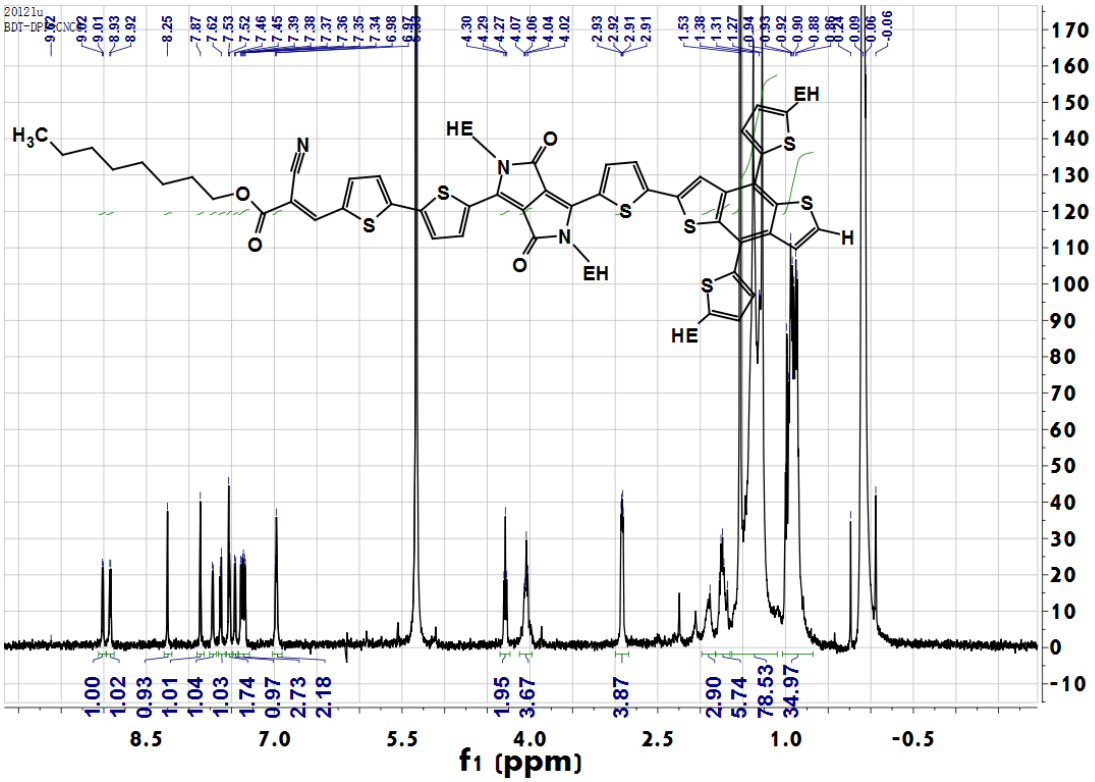

Figure S10. ^{1}H NMR spectrum of **M2**.

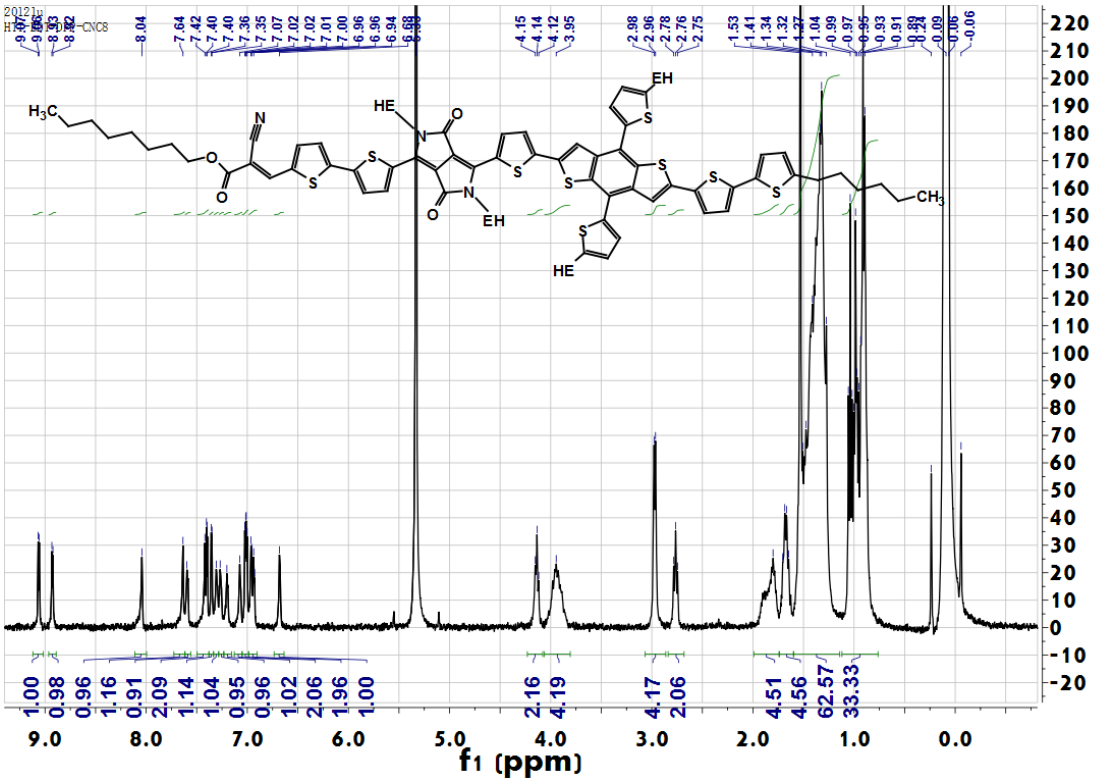

Figure S11. ^{1}H NMR spectrum of **M3**.

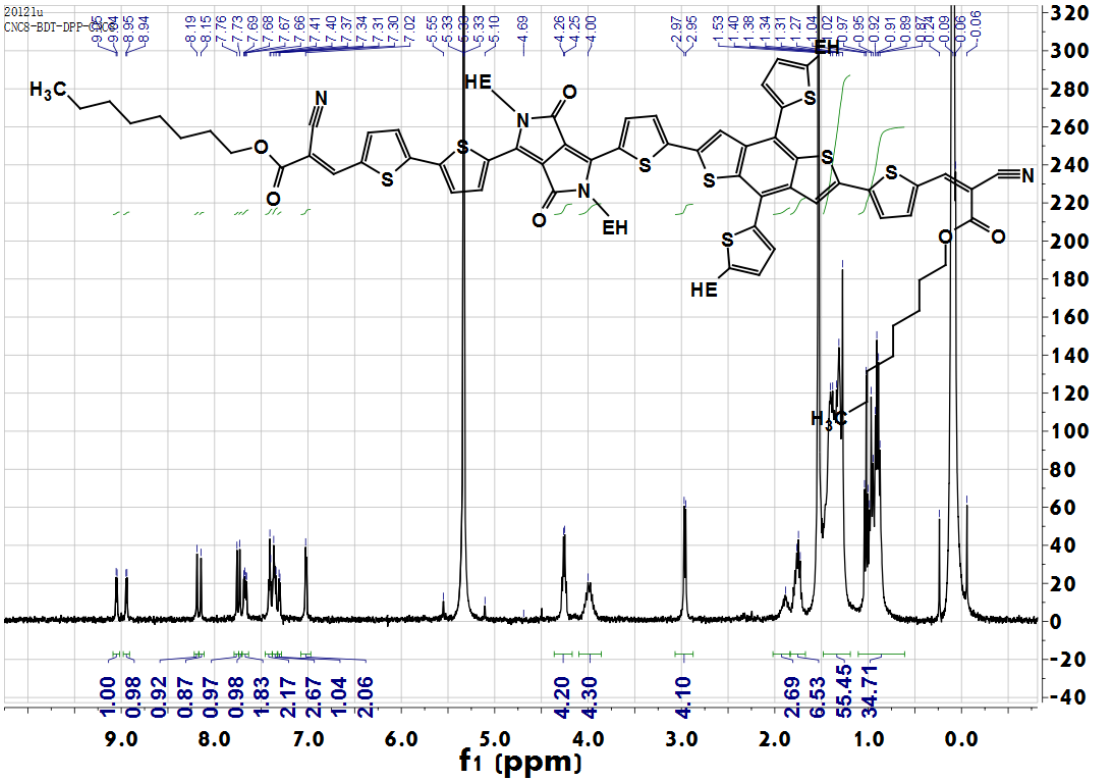

Figure S12. ^{1}H NMR spectrum of **M4**.

3. References

1. Z. H. Lu, B.Jiang, X. Zhang, A. L. Tang, L. L. Chen, C. L. Zhan and J. N. Yao, *Chem. Mater.* 2014, **26**, 2907–2914.
2. M. J. Frisch, G. W. Trucks, H. B. Schlegel, G. E. Scuseria, M. A. Robb, J. R. Cheeseman, J. A. Montgomery Jr., T. Vreven, K. N. Kudin, J. C. Burant, J. M. Millam, S. S. Iyengar, J. Tomasi, V. Barone, B. Mennucci, M. Cossi, G. Scalmani, N. Rega, G. A. Petersson, H. Nakatsuji, M. Hada, M. Ehara, K. Toyota, R. Fukuda, J. Hasegawa, M. Ishida, T. Nakajima, Y. Honda, O. Kitao, H. Nakai, M. Klene, X. Li, J. E. Knox, H. P. Hratchian, J. B. Cross, V. Bakken, C. Adamo, J. Jaramillo, R. Gomperts, R. E. Stratmann, O. Yazyev, A. J. Austin, R. Cammi, C. Pomelli, J. W. Ochterski, P. Y. Ayala, K. Morokuma, G. A. Voth, P. Salvador, J. J. Dannenberg, V. G. Zakrzewski, S. Dapprich, A. D. Daniels, M. C. Strain, O. Farkas, D. K. Malick, A. D. Rabuck, K. Raghavachari, J. B. Foresman, J. V. Ortiz, Q. Cui, A. G. Baboul, S. Clifford, J. Cioslowski, B. B. Stefanov, G. Liu, A. Liashenko, P. Piskorz, I. Komaromi, R. L. Martin, D. J. Fox, T. Keith, M. A. Al-Laham, C. Y. Peng, A. Nanayakkara, M. Challacombe, P. M. W. Gill, B. Johnson, W. Chen, M. W. Wong, C. Gonzalez, and J. A. Pople, (Gaussian 03, Revision C.02, Gaussian, Inc., Wallingford CT, 2004).
3. A. D. Becke, *J. Chem. Phys.* 1993, **98**, 5648–5652.
4. A. D. Becke, *Phys. Rev. A* 1988, **38**, 3098–3100.
5. C. T. Lee, W. T. Yang, R. G. Parr, *Phys. Rev.* B 1998, **37**, 785–789.
6. M. A. Naik, N. Venkatramaiah, C. Kanimozhi, S. Patil, *J. Phys. Chem. C* 2012, **116**, 26128–26137
7. T. Y. Chu, O. K. Song, *Appl. Phys. Lett.* 2007, **90**, 203512(1)–203512(3).

8. J. Choi, C. Kim, J. Pison; A. Oyedele, D. Tondelier, A. Leliege, E. Kirchner, P. Blanchard, J. Roncali, B. Geffroy, *RSC. Adv.* 2014, **4**, 5236–5242.
9. C. Zhan, D. Wang, *J. Photochem. Photobiol.* A. 2002, **147**, 93–101.